JOURNAL OF CATALYSIS 135, 576–595 (1992)

# The Relationship between Catalyst Morphology and Performance in the Oxidative Coupling of Methane

JUSTIN S. J. HARGREAVES,* GRAHAM J. HUTCHINGS,* RICHARD W. JOYNER,* AND CHRISTOPHER J. KIELY†

*Leverhulme Centre for Innovative Catalysis, Department of Chemistry, and †Department of Materials Science and Engineering, University of Liverpool, PO Box 147, Liverpool L69 3BX, United Kingdom

Received August 19, 1991; revised December 9, 1991

A detailed study of the oxidative coupling of methane over magnesium oxide and lithium-doped MgO catalysts is presented. The morphology of a number of different catalysts has been examined by detailed transmission electron microscopy and the results have been correlated with catalyst performance, in particular selectivity to $C_2$ hydrocarbons. Three samples of magnesium oxide have been prepared by different methods. Magnesium oxides prepared from the hydroxide, (ex OH), and from burning magnesium ribbon in air show similar morphology, exposing largely {100} planes; they also show very similar catalytic selectivity and specific activity. The ribbon residue material, however, has a cube length which is greater than that of the ex OH material by a factor of 5–10. Steps and corner sites are therefore present in much greater density on the ex OH sample than on the ribbon residue, and, since catalyst performance is unchanged, it is clear that these sites play no significant part in the catalysis over these materials. The active site is therefore located on the planar {100} surfaces. The most selective magnesium oxide catalyst was prepared by thermal decomposition of magnesium hydroxycarbonate and exposed a greater proportion of higher index mean crystal planes, e.g., {111}, than the less selective forms of magnesium oxide. It is suggested that an additional selective site is present in this form of magnesium oxide, with density related to morphology but not directly to surface area, perhaps a "bottom step" site. The morphology/performance relationship has also been examined for lithium-doped magnesium oxide catalysts. In agreement with previous studies, addition of lithium causes a loss of surface area and of the morphology characteristic of the precursor magnesium oxide; the grain size also increases, grain boundary dislocations become evident, and dislocations are also observed in the bulk of the grains. These are immobile and of the type $\frac{1}{2}\langle 110\rangle$, pinned by the presence of lithium ions. The emergence of a dislocation at the surface of the crystallite provides a locus for $[Li^+O^-]$ centres, thought to be the active site in methyl radical generation in methane coupling. Similar dislocations are observed in Au/MgO catalysts, which are much less selective to $C_2$ hydrocarbons than is pure MgO. 

## INTRODUCTION

The instability of the crude oil price as a result of geopolitical considerations has recently highlighted the requirement for suitable alternative technologies to those based on oil. One such possible process is the oxidative coupling to methane to produce $C_2$ hydrocarbons. Considerable research interest has been given to this topic, since many large deposits of natural gas are found in remote locations (*1, 2*). Early work concentrated on the identification of suitable catalytic materials, and virtually all oxides display some catalytic activity for this reaction (*3–14*).

A number of studies have considered aspects of the reaction mechanism and considerable attention has been directed at the complex homogeneous/heterogeneous nature of the reactions involved (*15–17*). In general, it is considered that methane undergoes homolytic activation at the catalyst surface, with the generation of a methyl radical, and studies of the isotope effect have suggested that this step is rate determining



0021-9517/92 $5.00

for Li/MgO catalysts (*18*). The subsequent reactions of the methyl radicals occur primarily in the gas phase (*15–17, 19, 20*).

To date, very limited attention has been given to the importance of catalyst morphology for this reaction or to searching for structure sensitivity. Early studies on $Sm_2O_3$ catalysts indicated that different crystal structures could give rise to different catalytic performances (*21, 22*). More recently it has been demonstrated that the morphology of $La_2O_3$ has an important effect on the catalytic performance for methane activation (*23*). Lunsford *et al.* have concluded that the morphology of magnesium oxide does not influence its catalytic performance or that of lithium-doped catalysts (*24*). The lack of interest in structural aspects of coupling catalysts is somewhat surprising, in view of the generally accepted importance of surface structure and surface defects in a number of oxidation reactions (*25*). In this paper we present a detailed study of the effects of catalyst morphology for MgO and Li/MgO catalysts.

The morphology of magnesium oxide, which has the sodium chloride crystal structure, has been well studied (*26–28*). Electrostatic considerations dictate that the only stable, exposed surface is the {100} face, which contains equal quantities of magnesium and oxygen ions. Magnesium oxide crystallites are thus typically aggregates of small cubes, perhaps 50–100 Å in length, each exposing only the {100} face. When other crystal planes are apparently present, they are made up of {100} microfacets. Thus the {100} plane is built up of very long but narrow steps and terraces of {100} structure, with many four-coordinate atoms, while the mean {111} surface offers many corner three-coordinate sites. In contrast to zinc oxide, for example, differences in catalytic performance between different samples may result, not from the different structures of different surface planes, but from the relative numbers of magnesium and oxygen ions at corners and edges and in flat planes.

Quite large, nearly perfect cubes of magnesium oxide can be prepared by burning magnesium ribbon in air, and in this study these are compared with magnesium oxide from two other sources, namely decomposition of a basic carbonate and of a magnesium hydroxide. The latter two methods give much less ordered forms of magnesium oxide. In addition, the effect of Li doping is also described and we demonstrate that the morphological features of MgO and Li/MgO are of considerable importance with respect to the catalytic efficacy of these oxides for the oxidative coupling of methane.

## EXPERIMENTAL

### *Catalyst Preparation*

*Magnesium oxide catalysts.* Magnesium ribbon (99%, Aldrich) was burned in air and the resultant powder is referred to as "ribbon residue," or RR. The white ash was collected and heated in static air at 800°C for 24 h to destroy any magnesium nitride. This catalyst could only be tested in powder form.

Magnesium hydroxide (Merck, ultrapure) was calcined in static air at 450°C for 24 h and subsequently at 800°C for 24 h. Prior to calcination the magnesium hydroxide was pelleted without addition of binder and sieved to give particles to size 600–1000 $\mu$m. The resultant material is referred to as "ex OH."

Magnesium hydroxycarbonate (Merck, heavy, extrapure) was suspended in distilled water (750 ml), stirred at 70–90°C for 30 min, and then filtered and dried at 150°C for 16 h. The resulting material was pelleted without addition of binder, sieved (600–1000 $\mu$m), and calcined at 450°C for 24 h in static air, and at either 800 or 1100°C for a further 24 h. These materials are referred to respectively as "ex BC (800)" and "ex BC (1100)."

*Lithium-doped magnesium oxide catalysts.* To prepare ca. 5% $Li_2CO_3$/MgO, lithium carbonate (0.25 g, AR, BDH) was dissolved in distilled water (40 ml) with cooling.

MgO ex BC (800) or ex OH (5.00 g) was then impregnated with the lithium carbonate solution using a number of impregnation and drying stages. The resultant material was dried at 150°C for 16 h and then calcined in static air at 800°C for 3 h.

*Gold-doped magnesium oxide catalysts.* Au/MgO ca. 0.65% was prepared by impregnating MgO ex OH (5.00 g) with an aqueous solution of chloroauric acid (0.06 g/20 ml water, Johnson-Matthey). The resultant mixture was dried at 150°C for 16 h and then calcined at 800°C in static air for 3 h.

### *Catalyst Characterisation*

Elemental compositions were determined using inductively coupled plasma optical emission spectroscopy (ARL 3520 sequential spectrometer) and the results are given in Table 1. Surface areas were determined by nitrogen physisorption using a Micromeritics ASAP 2400 instrument. Transmission electron microscopy (TEM) was performed using a Philips 400T electron microscope operating at 120 kV in combination with a VG501 STEM. Two imaging techniques were used throughout this study, namely phase contrast to delineate surface details and diffraction contrast to show microstructural features, e.g., dislocations and grain boundaries. Two types of specimen preparation, according to the imaging technique utilised, were performed. For phase contrast micrographs (Fig. 1b), the sample was ultrasonically dispersed in Arklone and then applied to a copper support grid (Agar Scientific, 200 mesh, 3.05 mm diameter). The grid was dried in air prior to use. For other micrographs, the samples were prepared by sprinkling dry catalyst powder onto a carbon-coated copper support grid (Agar Scientific) and removing the excess by shaking.

### *Catalyst Testing*

Catalyst were evaluated for the oxidative coupling of methane using a fixed-bed laboratory microreactor constructed from quartz glass. The method of catalyst testing has previously been described (*29*), using a catalyst bed mass of 2.0 g and on-line gas chromatographic analysis. The gas composition was 46% $CH_4$, 8% $O_2$, balance helium, and the reaction was carried out at 1 bar total pressure and $T$ = 750°C unless otherwise stated, with the gas flow adjusted so that the oxygen conversion was in the range 95–99%. When hydrogen production was being measured, an argon diluent and carrier was used and the analysis was carried out off line. At the reaction conditions used, a negligible reaction was observed in an empty tube (oxygen conversion <2% at 750°C).

TABLE 1

ICP Analysis of MgO Catalysts

| Catalyst | Metal ion concentration (wt%)[a] | | | | | | |
|---|---|---|---|---|---|---|---|
| | Al | Ca | Fe | Ni | Na | K | Li |
| MgO ribbon residue | 0.05 | 0.03 | 0.02 | 0.11 | <0.01 | <0.01 | 0 |
| MgO ex BC (800) | 0.03 | 0.24 | 0 | 0 | 0.06 | 0 | 0.01 |
| MgO ex OH | 0.02 | 0.01 | 0 | 0 | 0 | 0 | 0 |
| MgO ex BC ($H_2O$) | <0.05 | 0.26 | <0.01 | <0.02 | 0.06 | <0.01 | 0 |
| Li/MgO ex BC | 0.01 | 0.23 | 0 | 0 | 0.06 | 0 | 0.63 |
| Li/MgO ex OH | 0.01 | 0.01 | 0 | 0 | 0.01 | 0.01 | 0.56 |

[a] Cu, Ti, and Zn all below limit of detection, ca. 0.01%.

The data were calculated in the following way:

$$CH_4 \text{ conversion } (\%) = 100 \cdot \Sigma(nC_n)/CH_{4_{in}},$$

where $C_n$ is the molar yield of carbon-containing products possessing $n$ carbon atoms and $CH_{4_{in}}$ is the mol% $CH_4$ in the reactor feed.

$$O_2 \text{ conversion } (\%) = 100 \cdot (O_{2_{in}} - O_{2_{out}})/O_{2_{in}},$$

where $O_{2_{in}}$ and $O_{2_{out}}$ are mol% $O_2$ in reactor feed and product gas streams, respectively.

$$\text{Selectivity } (\%) = 100 \cdot nC_n/\Sigma nC_n,$$

where the molecule contains $n$ carbon atoms.

## RESULTS

### *Electron Microscopy*

*MgO ribbon residue.* Electron micrographs of MgO ribbon residue after use as a catalyst are shown in Fig. 1. As expected, the crystallites in these micrographs exhibit cubic morphology and predominantly expose large {100} faces. The average side length of the cubes is ca. 1000–2000 Å and there is a fairly broad size distribution, as has been noted in previous studies of magnesium oxide smoke (*26*).

Phase contrast transmission electron microscopy allows surface detail to be studied. This technique was used to obtain Fig. 1b and it is apparent that the corners of the crystallites are rounded.

All samples of MgO, irrespective of their preparation method, were examined before and after use as catalysts for methane coupling and no changes in morphology were observed.

*MgO from the hydroxide.* The crystallites of magnesium oxide prepared by the thermal decomposition of magnesium hydroxide are shown in Fig. 2; their size is ca. 200–400 Å. In many cases there appears to be some degree of crystallite alignment, with the {100} face predominantly exposed, as is observed for the ribbon residue sample. Some noncrystalline regions were also observed for this material. The structure is consistent with previous studies of decomposed brucite (magnesium hydroxide) (*30, 31*).

*MgO from the basic carbonate.* The crystallites of ex BC (800) MgO shown in Fig. 3 are similar to those obtained from the hydroxide (Fig. 2). They are smaller and exhibit a less regular shape than those for the MgO ribbon residue (Fig. 1). The average size is ca. 200–400 Å. Samples prepared by calcination of magnesium hydroxycarbonate have been previously studied using TEM by Moodie and Warble (*26*), who obtained very similar micrographs. Ex BC (800) MgO exhibits a greater preponderance of microfacetted, higher index planes (e.g., {111} and {110}) than are observed with the MgO ribbon residue sample.

The influence of calcining the ex BC material at 1100°C is shown in Fig. 4. The crystallites now show similar morphology to the ribbon residue sample (Fig. 1), and the average crystallite size has increased to ca. 2000–4000 Å.

*Water-treated samples.* To assess the possible role of impurities in the catalysts, both ex hydroxide and ex basic carbonate materials were treated with distilled water, using the impregnation technique described above for the preparation of lithium-doped catalysts. Electron micrographs are shown in Fig. 5 (ex OH) and Fig. 6 (ex BC) and the samples are referred to as "ex OH ($H_2O$)" and "ex BC ($H_2O$)." In both cases this impregnation changes morphology and increases surface area (cf. Table 6), although the changes are more marked for the ex BC material, which now resembles the original ex OH morphology.

The ex BC material after water treatment displays a higher preponderance of {100} planes when compared with its precursor (see Fig. 3). The structure of the ex OH ($H_2O$) sample (Fig. 5) is consistent with previous observations of decomposed brucite (magnesium hydroxide) (*30, 31*). Both ex BC ($H_2O$) and ex OH ($H_2O$) samples are

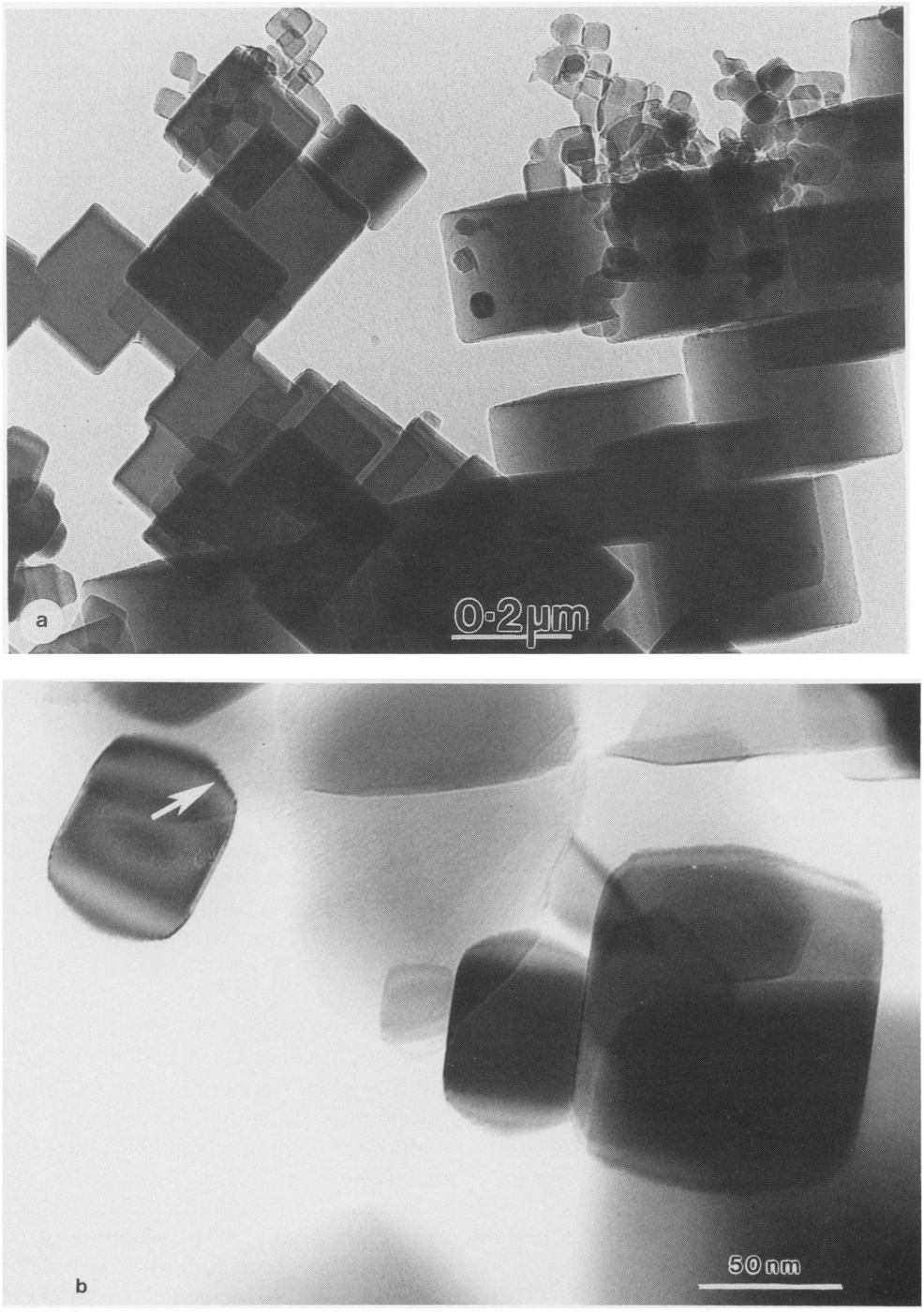


FIG. 1. (a) Transmission electron micrograph of MgO ribbon residue (noncalcined) after use as a coupling catalyst. Note the predominant cube morphology of the crystallites and the rounding off of the cube corners. (b) Phase contrast electron micrograph of MgO ribbon residue after use as a coupling catalyst. A high index surface composed of {100} type microsteps is arrowed.

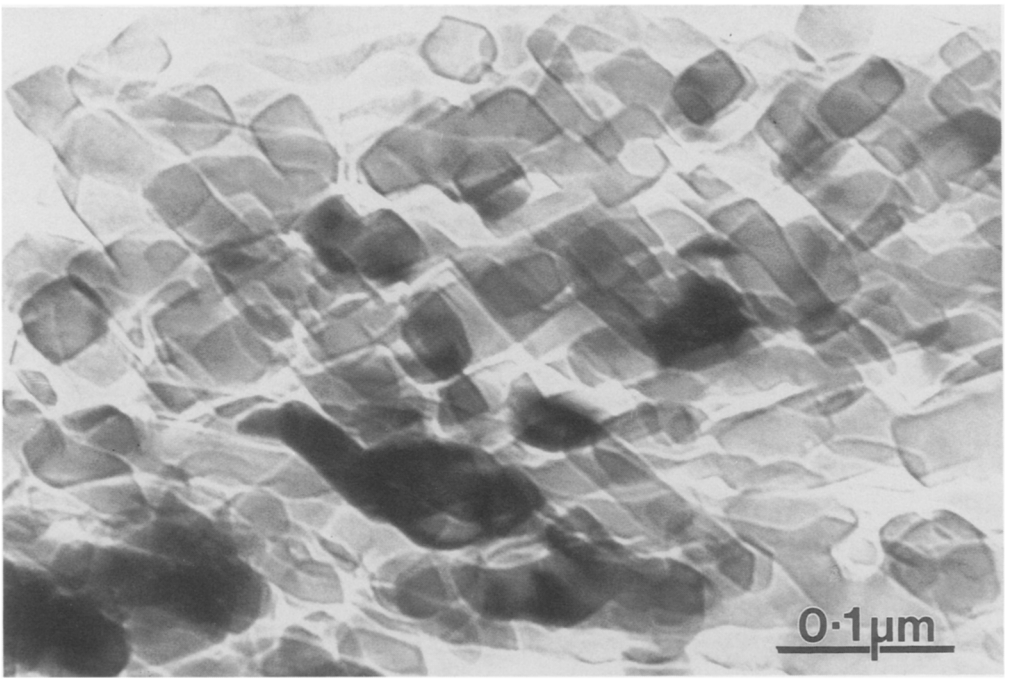


FIG. 2. Transmission electron micrograph of MgO ex OH prior to use as a coupling catalyst. Note the distinctive "blocky" morphology of the individual crystallites.

composed of hexagonal disc structures; the substructure apparent within the hexagonal discs is possibly a result of the process of forming polycrystals, which occurs when $Mg(OH)_2$ is decomposed.

*Lithium-doped magnesium oxide.* Representative micrographs of the lithium-doped samples, prepared from ex OH and ex BC precursors, are shown in Figs. 7 and 8. In contrast to the magnesium oxide samples, the morphologies of the two lithium carbonate-doped catalysts are similar. A number of features are observed, common to both types of lithium carbonate-doped catalyst.

(i) Compared to the parent magnesium oxide, the doped catalysts show a large increase of the catalyst particle size, which is consistent with the observed decrease in surface area (Table 7). The average grain diameter for the unused sample is ca. 2000–4000 Å in both cases. During catalyst use the grain growth continues, the average size rising to 3000–5000 Å, but without any significant morphological modification. The grain growth is probably a consequence of oxygen vacancies being introduced in order to maintain charge balance when $Li^+$ substitutes for $Mg^{2+}$. The presence of such vacancies facilitates diffusion within the lattice, thereby aiding the sintering process.

(ii) The grains have lost the shape characteristics of hydroxycarbonate or hydroxide precursors. In many cases the shape has become almost spherical, exposing mean higher index planes.

(iii) Examination of polycrystalline electron diffraction ring patterns of these materials showed no evidence for second phase formation, confirming that cubic magnesium oxide was the major phase present.

(iv) Irregular grain boundary dislocation arrays were observed (see Fig. 7).

(v) Dislocations are also observed in the bulk of the grains, which by systematic dislocation contrast imaging were identified to be predominantly of the type $\frac{1}{2}\langle 110\rangle$ (*32*).

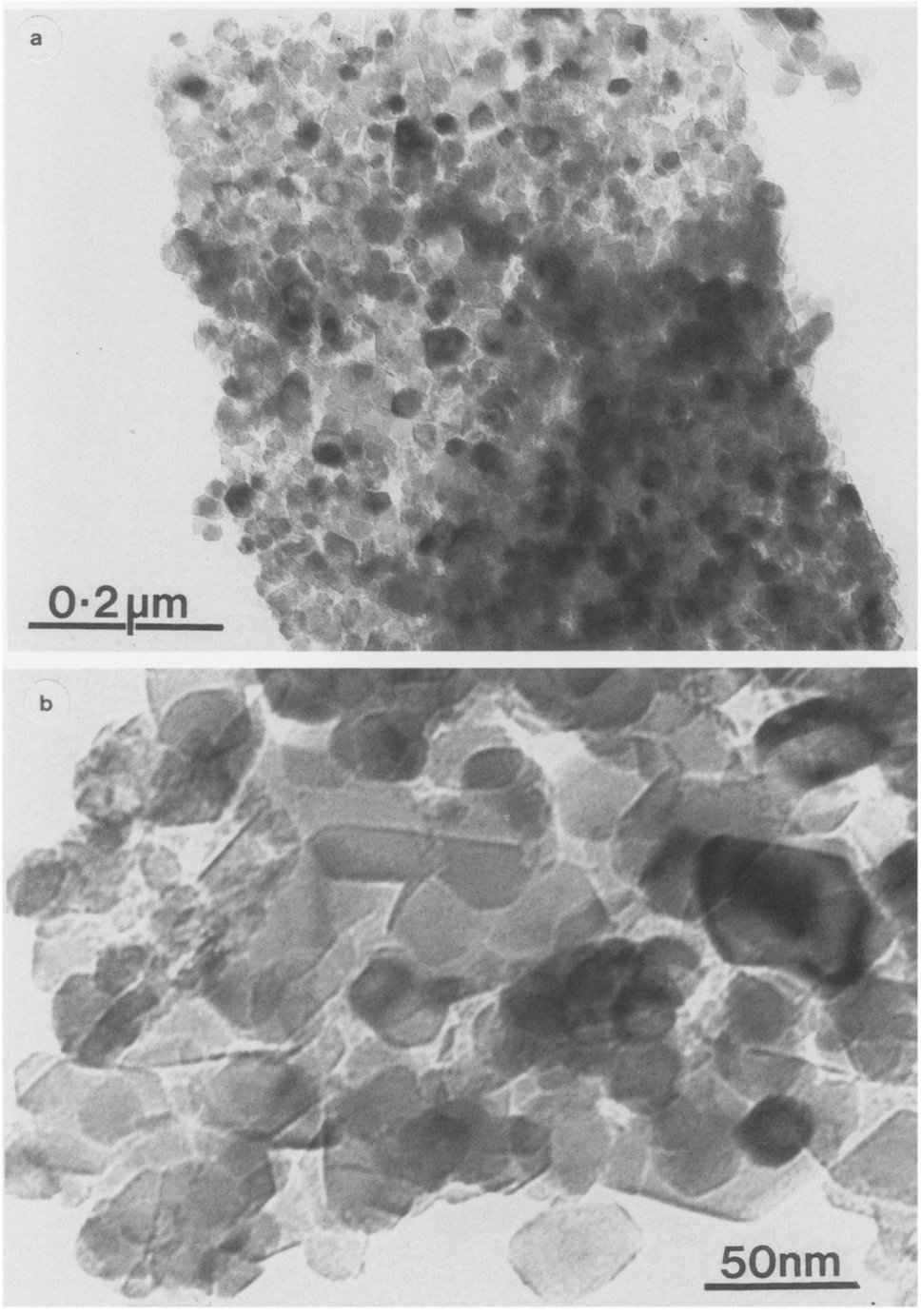


FIG. 3. (a) Low magnification electron micrograph of MgO ex BC (800) calcined in reaction atmosphere. (b) High magnification transmission electron micrograph of MgO ex BC (800) calcined in reaction atmosphere. The individual crystallites are now seen to be much more irregularly shaped.

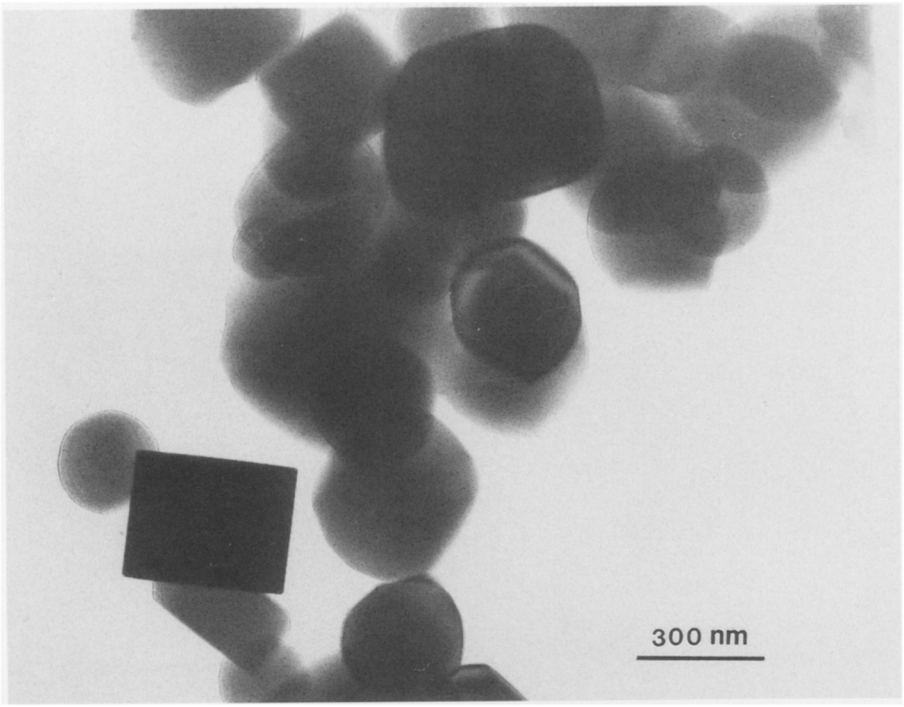


FIG. 4. Transmission electron micrograph of MgO ex BC (1100) prior to use as a coupling catalyst.

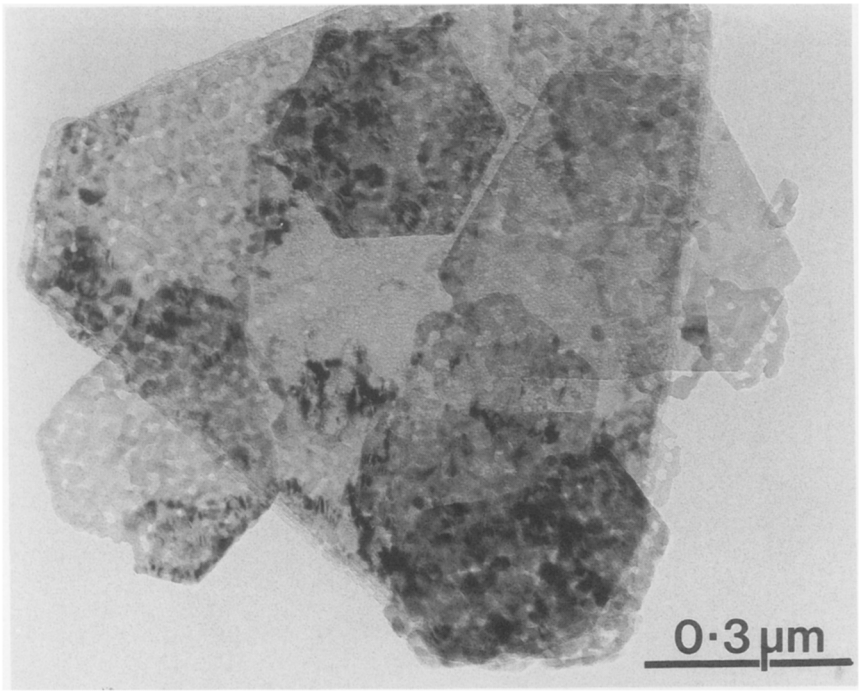


FIG. 5. Transmission electron micrograph of a wet impregnated MgO ex OH prior to use as a coupling catalyst. The crystallites are now arranged so as to form hexagonal platelets.

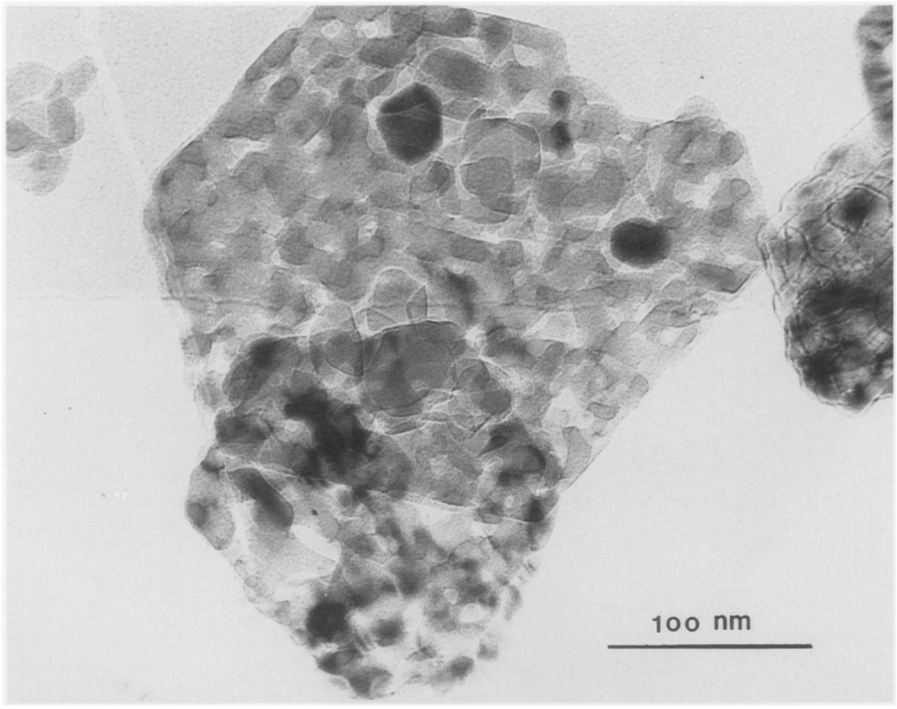


FIG. 6. Transmission electron micrograph of wet impregnated MgO ex BC (800) prior to use as a coupling catalyst.

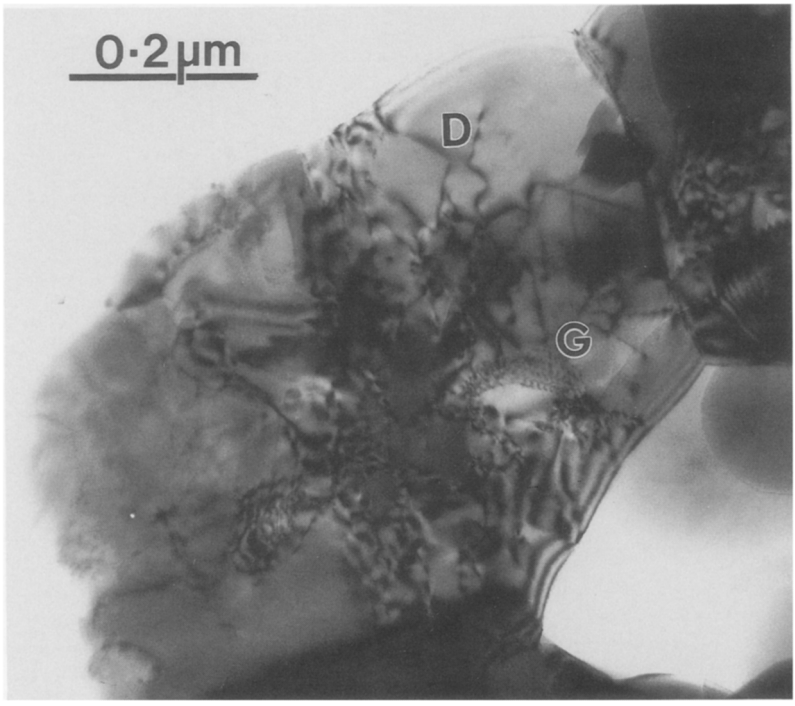


FIG. 7. Electron micrograph of ca. 5 wt% $Li_2CO_3$ doped MgO ex OH prior to use as a coupling catalyst. A grain boundary dislocation array (labelled G) and individual dislocations within the bulk of the crystal (labelled D) are clearly visible.

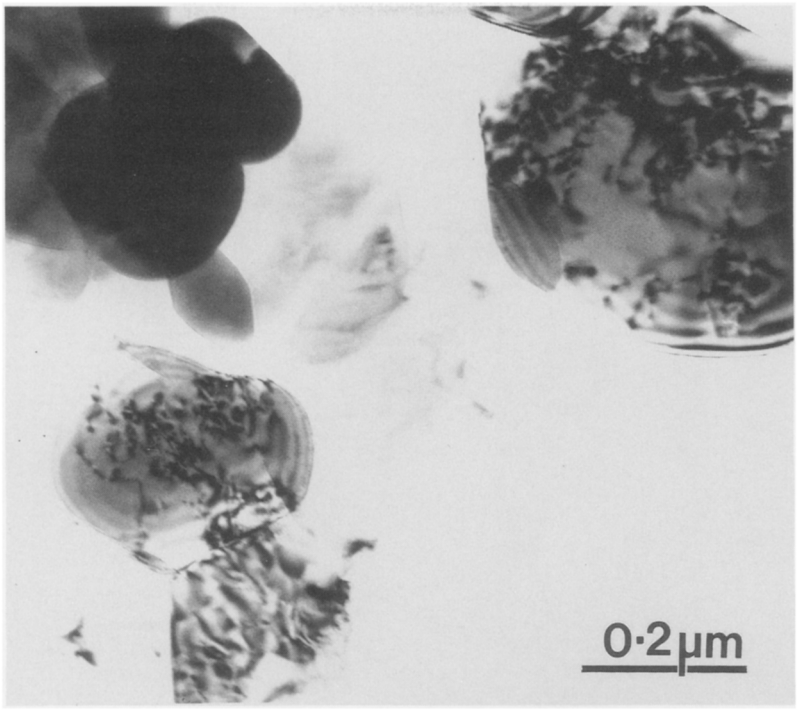


FIG. 8. Electron micrograph of ca. 5 wt% $Li_2CO_3$ doped MgO ex BC (800) after use as a coupling catalyst. Again, notice the dislocations present within individual grains.

Examples of this are shown in Figs. 7 and 8. These are not annealed out by high-temperature treatment and are immobile under electron beam irradiation, suggesting that they might be pinned by lithium segregation to the dislocation core.

(vi) During analysis of samples in the VG501 STEM instrument, mobile surface films were observed on many grains, which may contain lithium salts.

(vii) No evidence was found for the presence of lithium oxide inclusions in the used or unused samples. In addition, no $Li_2O$ was observed in a sample of magnesium oxide that had been calcined for 3 h at 1000°C (average grain size 9000 Å). This is in contrast to the observation of Narayan *et al.* (*33*), of $Li_2O$ large precipitates in bulk MgO crystallites, for 5% lithium carbonate-doped samples prepared by arc fusion and heated to 1200°C.

*Gold-doped magnesium oxide catalysts.* Representative micrographs of the Au/MgO sample are shown in Fig. 9. By comparison with the micrographs of the undoped ex OH material (Fig. 2), it is apparent that doping with gold has not changed the crystallite size significantly. However, the crystal morphology is less regular than that of ex OH MgO and in addition, $\frac{1}{2}\{110\}$ dislocations are apparent, which again seemed to be pinned in position. In this respect the morphology and dislocation behaviour of Au/MgO is similar to that of lithium-doped MgO (Figs. 7 and 8). No evidence for metallic gold particles was found, suggesting that the gold is present in a highly dispersed form.

### *Catalyst Performance in the Oxidative Coupling of Methane*

*Magnesium oxide catalysts.* Three different preparations of magnesium oxide were investigated for the oxidative coupling of methane at 750°C, and the results are shown

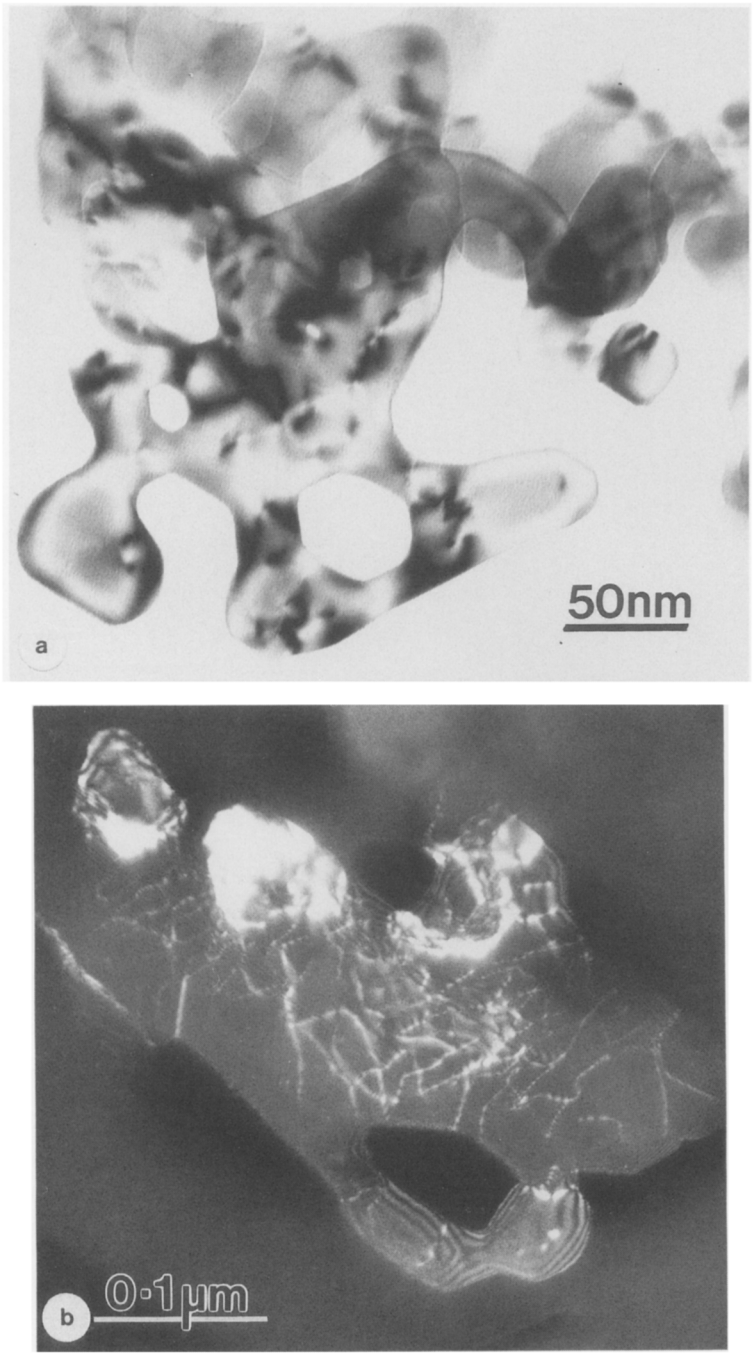


FIG. 9. (a) A bright field transmission electron micrograph of an unused Au/MgO catalyst. Dislocation contrast is once more in evidence. (b) Weak beam micrograph taken in a $g = 220$ reflection showing dislocation tangles within a grain of unused Au/MgO catalyst.

TABLE 2

Oxidative Coupling of Methane at 750°C over Magnesium Oxide Catalysts Prepared by Different Methods

| Catalyst | Surface area[e] ($m^2 \cdot g^{-1}$) | GHSV ($h^{-1}$) | $CH_4/O_2$ | Conversion (%) | | Product selectivity (%) | | | | | $(C_2H_6 + C_2H_4)/(CO + CO_2)$ |
|---|---|---|---|---|---|---|---|---|---|---|---|
| | | | | $CH_4$ | $O_2$ | $C_2H_6$ | $C_2H_4$ | CO | $CO_2$ | $H_2$ | |
| MgO ribbon | 5.2 | 714 | 5.5 | 13.8 | 97.0 | 18.6 | 10.0 | 18.0 | 53.4 | 9.6 | 0.40 |
| residue[a] | 5.2 | 1429 | 5.4 | 12.4 | 85.9 | 20.9 | 8.4 | 21.3 | 49.4 | — | 0.41 |
| MgO ribbon | 5.2 | 1500 | 5.3 | 14.1 | 92.7 | 18.3 | 9.8 | 20.5 | 51.4 | 9.3 | 0.39 |
| residue[b] | 5.2 | 3000 | 5.4 | 10.9 | 66.9 | 19.4 | 7.0 | 31.1 | 42.5 | 14.8 | 0.36 |
| | 5.2 | 6000 | 5.5 | 9.8 | 51.9 | 21.9 | 6.4 | 37.6 | 34.1 | 16.7 | 0.39 |
| MgO ex | 21 | 882 | 5.9 | 17.1 | 99.4 | 26.3 | 23.4 | 9.4 | 40.9 | 19.9 | 0.99 |
| BC (800)[c] | 21 | 1765 | 5.6 | 18.3 | 100 | 29.2 | 20.7 | 12.2 | 37.9 | — | 1.00 |
| | 21 | 3529 | 5.5 | 19.2 | 100 | 30.6 | 19.2 | 16.8 | 33.4 | — | 0.99 |
| | 21 | 7059 | 5.5 | 23.2 | 97.8 | 31.9 | 31.1 | 14.7 | 22.3 | 13.5 | 1.70 |
| MgO ex OH[d] | 32 | 1000 | 5.5 | 15.8 | 99.4 | 15.7 | 14.2 | 24.3 | 45.8 | 21.6 | 0.43 |
| | 32 | 2000 | 5.6 | 16.3 | 98.1 | 16.6 | 11.8 | 28.2 | 43.4 | 21.5 | 0.40 |

[a] 2.03 g MgO ribbon residue, volume = 4.2 ml; [b] 1.01 g MgO ribbon residue, volume = 2.0 ml; [c] 2.04 g MgO ex BC (800), volume = 3.4 ml; [d] 2.04 g MgO ex OH, volume = 3.0 ml; $CH_4$ : diluent 1 : 1, temperature 750°C, pressure 101 kPa.

[e] Refers to materials before use.

in Table 2. At comparable reaction conditions the ex BC (800) material is more selective to $C_2$ hydrocarbons and is somewhat more active than the other two samples, which have similar catalytic performance. The three samples have different surface areas and precise activity comparison is therefore difficult, since coupling is known to involve a combination of surface and gas phase chemistry (*15–17*). Table 2 demonstrates that total selectivity to $C_2$ hydrocarbons does not depend markedly on space velocity, which is representative of residence time in the reactor.

It was not possible to pelletise the ribbon residue sample, which was therefore studied in powder form. To test if the performance was influenced by particle size, ex BC (800) and ribbon residue samples were tested in powder form under the same reaction conditions. The results, shown in Table 3, indicate that the differences in selectivity remain. The oxygen conversions are not strictly comparable, but Table 2 shows that the combined $C_2$ selectivity of the ribbon residue is independent of oxygen conversion.

The effect of reaction temperature on the oxidative coupling of methane over an ex OH catalyst was investigated and the results are shown in Table 4. As noted for other coupling catalysts (*20*), methane conversion

TABLE 3

The Oxidative Coupling Performance of Powdered Magnesium Oxide Catalysts[a]

| Catalyst | GHSV ($h^{-1}$) | $CH_4/O_2$ | Conversion (%) | | Product selectivity (%) | | | |
|---|---|---|---|---|---|---|---|---|
| | | | $CH_4$ | $O_2$ | $C_2H_6$ | $C_2H_4$ | CO | $CO_2$ |
| MgO ex BC (800) | 1250 | 5.4 | 21.1 | 98.6 | 24.8 | 25.6 | 16.4 | 33.2 |
| MgO ribbon | 1500 | 5.3 | 14.1 | 92.7 | 18.3 | 9.8 | 20.5 | 51.4 |

[a] 1.01 g MgO ex BC (800), volume = 2.4 ml; 1.01 g MgO ribbon residue, volume = 2.0 ml; total flow rate 50 ml · $min^{-1}$; $CH_4$ : diluent 1 : 1; temperature 750°C, pressure 101 kPa.

TABLE 4

Temperature Dependence of Oxidative Coupling Performance of Magnesium Oxide Catalysts[a]

| Catalyst | Surface area ($m^2 \cdot g^{-1}$) | GHSV ($h^{-1}$) | Temp. (°C) | $CH_4/O_2$ | Conversion (%) | | Product selectivity | | | |
|---|---|---|---|---|---|---|---|---|---|---|
| | | | | | $CH_4$ | $O_2$ | $C_2H_6$ | $C_2H_4$ | CO | $CO_2$ |
| Mg ex OH | 32 | 938 | 700 | 5.5 | 14.6 | 93.8 | 10.0 | 5.1 | 38.9 | 46.0 |
| | | 938 | 750 | 5.5 | 16.8 | 99.8 | 16.0 | 14.8 | 24.8 | 44.4 |
| | | 938 | 800 | 5.5 | 18.8 | 100 | 19.1 | 24.2 | 16.1 | 40.6 |
| MgO ex BC (800 *in situ*) | 29 | 682 | 720 | 5.7 | 14.5 | 100 | 22.8 | 15.4 | 7.4 | 54.3 |
| | | 682 | 750 | 5.7 | 15.7 | 100 | 24.7 | 21.0 | 7.5 | 46.8 |
| | | 682 | 800 | 5.7 | 19.9 | 100 | 21.1 | 26.9 | 10.3 | 41.7 |

[a] 2.04 g (3.2 ml) MgO ex OH; 2.00 g MgO ex BC (800, *in situ*); $CH_4$ : diluent 1 : 1; flow rate 50 ml · $min^{-1}$; pressure 101 kPa.

and combined $C_2$ selectivity both increase with temperature. Table 4 demonstrates another general feature of the methane coupling reaction, namely that the ethene/ethane ratio increases with temperature. Table 4 also shows the performance of an ex BC catalyst which had been calcined only at 450°C before exposure to the reaction mixture. This procedure produces a higher surface area magnesium oxide but leads to a worse catalyst.

Although there are clear differences between the catalytic performance of different magnesium oxide samples, quantitative analysis indicates that there are also differences in the impurity content (Table 1). In particular, the ex BC (800) catalyst, which exhibits the best coupling performance, also contains the highest concentration of calcium and sodium impurities. Two approaches were adopted to normalise the contribution of impurities and to assess the importance of the catalyst morphology, viz. examining the role of calcination temperature and of treatment with water. The catalytic performance of the hydroxycarbonate-derived sample calcined at 1100°C (ex BC (1100)) is indicated in Table 5, which includes data for a ribbon residue catalyst for comparison. Calcination at 1100°C, when compared to that at 800°C, decreases the surface area of the resultant oxide considerably and the catalytic performance is signficantly changed; in particular the $C_2$ selectivity is decreased. Under conditions of similar oxygen conversion, the $C_2$ hydrocarbon selectivities of ex BC (1100) and ribbon residue are similar.

Treatment with water does not alter the impurity levels in the ex BC catalysts (Table 1) but does change the morphology, as can be seen by comparing Figs. 3 and 6. The performance of the resulting catalysts is given in Table 6, which shows that the selec-

TABLE 5

Effect of Calcination Temperature on the Catalytic Performance of MgO ex BC[a]

| Catalyst precursor | Surface area ($m^2 \cdot g^{-1}$) | GHSV ($h^{-1}$) | $CH_4/O_2$ | Conversion (%) | | Product selectivity (%) | | | |
|---|---|---|---|---|---|---|---|---|---|
| | | | | $CH_4$ | $O_2$ | $C_2H_6$ | $C_2H_4$ | CO | $CO_2$ |
| MgO ex BC (1100) | 3 | 1034 | 5.7 | 14.7 | 88.9 | 19.2 | 12.5 | 26.6 | 41.7 |
| MgO ribbon residue | 5 | 714 | 5.5 | 12.4 | 97.0 | 18.6 | 10.0 | 18.0 | 53.4 |

[a] 2.0 g catalyst, $CH_4$ : diluent 1 : 1; flow rate 50 ml · $min^{-1}$; 750°C, 101 kPa.

TABLE 6

Oxidative Coupling of Methane Over Magnesium Oxide Catalysts after Treatment with Water[a]

| Catalyst precursor | Surface area ($m^2 \cdot g^{-1}$) | GHSV ($h^{-1}$) | $CH_4/O_2$ | Conversion (%) | | Product Selectivity (%) | | | |
|---|---|---|---|---|---|---|---|---|---|
| | | | | $CH_4$ | $O_2$ | $C_2H_6$ | $C_2H_4$ | CO | $CO_2$ |
| MgO ex BC ($H_2O$) | 40 | 1000 | 5.5 | 17.1 | 100 | 19.8 | 14.7 | 18.5 | 47.0 |
| MgO ex BC (800) | 21 | 882 | 5.9 | 17.1 | 99.4 | 26.3 | 23.4 | 9.4 | 40.9 |
| MgO ex OH ($H_2O$) | 52 | 1034 | 5.7 | 14.7 | 100 | 13.5 | 10.6 | 25.4 | 50.5 |
| MgO ex OH | 32 | 1000 | 5.5 | 15.8 | 99.4 | 15.7 | 14.2 | 24.3 | 45.8 |

[a] 2.0 g catalyst, $CH_4$ : He 1 : 1; 750°C, 101 kPa.

tivity of the ex BC ($H_2O$) material falls to a value similar to that of the ex hydroxide catalyst.

*Lithium-doped MgO catalysts.* The oxidative coupling of methane was investigated for two samples of magnesium oxide doped with ca. 5 mass% $Li_2CO_3$, derived respectively from the hydroxycarbonate and the hydroxide and denoted Li/MgO ex BC and Li/MgO ex OH. The elemental analysis of these catalysts is given in Table 1 and the catalytic data are given in Table 7. The activities and selectivities of the two lithium-doped catalysts are very similar, although the MgO precursors were different. In agreement with numerous previous studies (*20*), the addition of lithium carbonate to MgO significantly decreases the surface area but increases both the specific activity and the selectivity for $C_2$ hydrocarbon production.

*Gold-doped MgO catalysts.* The oxidative coupling of methane was investigated for MgO ex OH doped with 0.65% by weight of gold, and the results are given in Table 8. Addition of gold markedly decreases the selectivity to $C_2$ hydrocarbons and somewhat reduces the activity, although the surface area also decreases. The major products with the Au/MgO catalyst are carbon oxides.

## DISCUSSION

### *Morphology/Function Relationship for Magnesium Oxide Catalysts*

The results presented show that magnesium oxide catalysts prepared by burning magnesium ribbon or from the hydroxide have similar performance in the oxidative coupling of methane at 750°C, which is different from that of the more selective, ex basic carbonate material. As can be seen from the figures, catalysts prepared by the different methods exhibit distinctly different morphologies but in no case is the morphology significantly changed by exposure to the reaction atmosphere at 750°C. This is perhaps surprising, in view of the presence of water and carbon dioxide, each of which

TABLE 7

Oxidative Coupling Performance of Lithium-Doped MgO Catalysts[a]

| Catalyst precursor | Surface area ($m^2 \cdot g^{-1}$) | GHSV ($h^{-1}$) | $CH_4/O_2$ | Conversion (%) | | Product selectivity (%) | | | | |
|---|---|---|---|---|---|---|---|---|---|---|
| | | | | $CH_4$ | $O_2$ | $C_2H_6$ | $C_2H_4$ | CO | $CO_2$ | $H_2$ |
| Li/MgO ex BC | 3 | 1667 | 5.5 | 23.9 | 98.8 | 36.1 | 36.1 | 0.4 | 27.4 | 5.2 |
| Li/MgO ex OH | 3 | 1667 | 5.5 | 25.2 | 98.9 | 35.8 | 37.6 | 0.3 | 26.3 | 5.1 |

[a] 2.0 g (1.8 ml) catalyst, $CH_4$ : diluent 1 : 1; 750°C, 101 kPa.

TABLE 8

The Oxidative Coupling Performance of Au/MgO and MgO ex OH Catalysts[a]

| Catalyst | Surface area[b] ($m^2 \cdot g^{-1}$) | GHSV ($h^{-1}$) | Temp. (°C) | $CH_4/O_2$ | Conversion (%) | | Product Selectivity (%) | | | |
|---|---|---|---|---|---|---|---|---|---|---|
| | | | | | $CH_4$ | $O_2$ | $C_2H_6$ | $C_2H_4$ | CO | $CO_2$ |
| Au/MgO | 21 | 1071 | 600 | 6.1 | 0.4 | 5.1 | 0 | 0 | 0 | 100 |
| | 21 | 1071 | 650 | 6.2 | 1.0 | 18.5 | 0 | 0 | tr | 100 |
| | 21 | 1071 | 700 | 6.3 | 4.3 | 41.9 | tr | tr | 40.9 | 59.1 |
| | 21 | 1071 | 750 | 6.4 | 7.4 | 67.9 | 5.5 | 2.5 | 36.1 | 55.9 |
| | 21 | 1071 | 800 | 5.9 | 10.3 | 95.9 | 7.2 | 5.1 | 27.0 | 60.7 |
| MgO ex OH | 32 | 938 | 700 | 5.5 | 14.6 | 93.8 | 10.0 | 5.1 | 38.9 | 46.0 |
| | 32 | 938 | 750 | 5.5 | 16.8 | 99.8 | 16.0 | 14.8 | 24.8 | 44.4 |
| | 32 | 938 | 800 | 5.5 | 18.8 | 100.0 | 19.1 | 24.2 | 16.1 | 40.6 |

[a] 2.04 g Au/MgO, volume = 2.8 ml; 2.04 g MgO ex OH, volume = 3.2 ml; $CH_4$ : diluent 1 : 1; total flow rate 50 ml · $min^{-1}$; pressure 101 kPa.
[b] Surface area of unused catalyst.

can etch magnesium oxide (*34*). The micrographs of the ribbon residue cubes (Fig. 1) show that there is some rounding of the corners during reaction, and it has been suggested (*34*) that water and carbon dioxide, when present together, etch MgO smoke to a significantly lesser extent than either component alone.

The catalysts have been tested under what have become accepted conditions for methane coupling (*20*), namely, near 100% oxygen conversion, so it is not easy to make meaningful specific activity comparisons. However, from studies with varying space velocity (*35*) it is known that there are only small differences in the specific rates of methane conversion among the catalysts, although the ex BC (800) catalyst appears somewhat more active than the ribbon residue material.

Table 2 shows that, where measurements at different space velocities have been made, the ratio of ethane to ethene increases with space velocity, as does that of carbon monoxide to carbon dioxide. However, for each catalyst the ratio

$$\frac{\text{(Total } C_2 \text{ hydrocarbons)}}{\text{(Total carbon oxides)}}$$

appears to be broadly independent of space velocity. The decrease in the ethene/ethane ratio as the space velocity increases is not unexpected, since we have shown elsewhere that ethene, from the thermal cracking of ethane, is a secondary product over magnesium oxide catalysts (*29, 35*). The amount produced is therefore expected to fall as the reactor residence time is decreased. Similarly carbon dioxide is a secondary product (*29, 35*) from the catalysed water gas shift reaction, and its production again falls with increasing space velocity. The constant ratio of $C_2$ hydrocarbons to carbon oxides for the RR and ex OH catalysts is thus of considerable mechanistic significance. Either there is only one type of active site, which catalyses formation of $C_2$'s and carbon oxides to the same extent, or there are equal numbers of two different sites on both catalysts, respectively responsible for coupling and total oxidation. In view of the very similar catalytic performances of RR and ex OH materials, we suggest that there is only a single catalytic site, which is responsible for both the selective and the nonselective reactions effected by the catalyst. While we cannot firmly rule out the possibility of two sites with equal numbers in both materials, this seems implausible, in view of the considerable differences in particle sizes. Evidence for the existence of only one type of site on magnesium oxide, in comparison to the two sites thought to be active on lithium-doped

oxides (*20, 36*), is also provided by a study of the effect of adding nitric oxide to the reaction (*37*). Addition of NO over MgO and Li/MgO during reaction is found to have different effects, which are indicative of the different natures of the active sites. For Li/MgO, NO causes an immediate decline in the production of $C_2$ hydrocarbons, together with a corresponding increase in $CO_2$. On removal of NO, $C_2$ hydrocarbon increases temporarily to a level significantly higher than that observed prior to NO addition. Such observations can be explained in terms of two active sites being present in Li/MgO. For MgO, no effect in $CO_2$ or promotion in $C_2$ hydrocarbon production was observed on removal of NO, although a slight decrease in $C_2$ hydrocarbons is observed on NO addition; these observations are more consistent with the presence of a single active site.

The ex OH and RR samples have similar morphologies, both exposing predominantly {100} faces. As noted in the Introduction, any structure sensitivity of different magnesium oxide samples is likely to reflect the different numbers of low-coordination sites present. Although ex OH and RR samples have similar morphologies, they have markedly different particle sizes and therefore will have different *absolute* and *relative* numbers of three-, four-, and five-coordinate ions. The cube size of the RR material is 1000–2000 Å, 5 to 10 times that of the ex OH material, which is 200–400 A. This difference is well reflected in the sixfold difference in surface areas. If both samples were composed of perfect cubes, the number density of three-coordinate corner sites in the ex OH material would be 100–1000 times that of the ex RR (between $5^3$ and $10^3$), while that of four-coordinate edge sites would be 25–100 times greater in the ex OH ($5^2$–$10^2$). The phase contrast and other diffraction contrast micrographs of the RR material show that the cubes which compose it are not perfect. However, comparison with the ex OH material indicates a much greater degree of perfection, so that the number of edge and corner sites *per unit area* is clearly less on the RR samples.

The conclusion to be drawn from this is obvious and interesting: the site involved in the rate-determining step on these two materials may not involve the lowest coordination, edge, or corner ions; otherwise, the ex OH catalysts would have a much greater specific activity. Similarly, the selectivity of these catalysts cannot be determined by the participation of these edge or corner sites. The active sites must instead be located either on the planar faces or at special sites whose numbers do not correlate with the crystallite size of the catalyst. The result that edge and corner sites do not play a significant role in methane coupling catalysis is at variance with the theoretical study of Mehandru *et al.* (*38*), which considered an $Mg_{21}O_{20}^{3+}$ cluster, corresponding to the presence of one $O^-$ species. These authors concluded that rougher magnesium oxide surfaces would promote less selective reactions via methyl radical oxidation associated with ion pairs containing $Mg_{3c}^{2+}$ species. If this were correct, we would expect the ex OH catalyst to be markedly less selective than the RR material.

There have been few detailed studies of the reaction mechanism over magnesium oxide, since most investigators have been concerned with the more selective lithium-doped catalyst. The consensus for Li/MgO is that methane reacts at oxygen vacancies on the catalyst surface to form methyl radicals, which desorb immediately, dimerising in the gas phase to form ethane. Carbon oxides result from subsequent interactions of methyl radicals or product molecules with the surface or in the gas phase. Activation of $CH_4$ on Li/MgO is thus a homolytic process, and the introduction of a radical scavenger, NO, significantly decreases methane conversion for this catalyst (*37*). For MgO, NO addition similarly was found to decrease $C_2$ hydrocarbon when oxygen was utilised as an oxidant (*37*), indicating that radical processes are also important for the undoped catalyst. It is probable that the mechanism

of methane activation is via methyl radicals in both systems and that methane activation on magnesium oxide occurs at oxygen vacancies on planar {100} surfaces.

The most selective magnesium oxide for the production of $C_2$ hydrocarbon was that prepared by thermal decomposition of the basic carbonate, as indicated in Table 2. This material comprises a large number of higher index mean crystal planes, e.g., {111}, whereas the less selective materials (ex hydroxide and ex ribbon residue) exposed mainly the {100} plane. Table 1, however, shows that the ex BC samples also have the highest concentration of calcium and sodium impurities, both of which have been shown to enhance the $C_2$ selectivity of magnesium oxide catalysts. Ex BC and ex OH catalysts have been studied by X-ray photoelectron spectroscopy, using a VG ESCA 3 spectrometer. In each case the surface concentrations of sodium and calcium were close to the limits of detectability, estimated at ~0.05% of a monolayer. These concentrations are much lower than those known to be necessary to enhance $C_2$ selectivities (*39*). Two additional types of experiment which change catalyst morphology without altering impurity content have been conducted, and each has shown that morphology, rather than impurity content, is responsible for the increased selectivity of the ex BC catalysts. Calcining the ex BC material at 1100°C rather than 800°C produced a material with morphology similar to that of the ribbon residue catalysts, as can be seen by comparing Figs. 3 and 4. The catalytic performance of the ex BC oxide also changed, resulting in both the selectivity and the activity becoming very similar to that of the RR catalyst, as can be seen from Table 5.

A sample of the ex BC 800 catalyst was treated with water, which changed both the morphology and the catalytic performance, as shown in Figs. 3 and 6 and Table 6. The morphology became similar to that of the ex OH catalyst, and at the same time the selectivity to $C_2$ hydrocarbons decreased. Since Table 1 shows that the impurity content of the ex BC (800) sample treated in this manner did not change, it can be seen that the morphology of the magnesium oxide is again the predominant influence in determining selectivity. Although it is always difficult to rule out any role for catalyst impurities, these studies suggest that the oxidative coupling reaction of methane over magnesium oxide is a structure-sensitive reaction.

What then is the nature of the active sites on the ex BC magnesium oxide? It should first be noted that the vacancy, point defects, which are active on the ex OH and RR catalysts, will still be present in the ex BC catalysts. We believe that the additional selectivity of the ex BC catalysts arises from a different, more selective site, present in greater numbers at the surface of the ex BC material because of its different morphology. The enhanced number of active sites may contribute to the much higher selectivity observed with MgO ex BC, since the gas phase concentration of $CH_3^{\cdot}$ will be increased, thereby giving higher probability of ethane formation via methyl radical coupling. Table 2 establishes that the specific activity of the ex BC material is greater than that of the RR catalysts. Under otherwise identical conditions the ex BC catalyst maintained close to 100% oxygen conversion at all space velocities studied up to 7000 $h^{-1}$. At a space velocity of 1500 $h^{-1}$ (equivalent to 6000 $h^{-1}$ for the higher area ex BC material), the oxygen conversion had already fallen to <93%. The ex BC catalysts have a much less regular morphology than the other two samples, as indicated in Fig. 3. As a result, the ratios of steps, edges, and corners to planar surfaces are much higher in this catalyst than in the others, so it is possible that these low-coordination sites are now present in sufficient numbers to contribute to catalyst performance. The greater proximity of these low-coordinate sites in the ex BC catalyst may also enhance $C_2$ selectivity. An alternative possibility is that the "bottom step" site, shown diagram-

matically in Fig. 10, is catalytically active. The irregular, quasi-spherical morphology of the ex BC material will result in the presence of a much greater number of this type of site, which are expected in only small numbers on the other catalysts studied.

*Morphology/Function Relationship for Lithium-Doped Magnesium Oxide Catalysts*

As others have observed, the addition of lithium carbonate to a magnesium oxide catalyst increases the specific activity for the oxidative coupling of methane and the selectivity of $C_2$ hydrocarbon formation (*20*). Previous studies have also shown that lithium carbonate doping of MgO leads to an increase in the grain size of the magnesium oxide crystallites (*24*). The micrographs in Figs. 7 and 8 show that sintering of the crystallites is accompanied by the loss of the regular morphology of the magnesium oxide precursor and by the formation of grain boundary dislocations. In agreement with Lunsford *et al.* (*24*), the morphology of the magnesium oxide precursor does not influence the performance of the lithium-doped catalysts, since both structure and reactivity are the same in Li/MgO catalysts prepared either from the ex hydroxide or from the ex basic carbonate precursor, as can be seen in Figs. 7 and 8 and Table 7.

Electron diffraction shows that cubic magnesium oxide is the only solid phase present, although there is also a mobile film, probably of lithium carbonate. No evidence is found for discrete precipitates of lithium oxide, which have been reported under some conditions (*33*), although not in methane coupling catalysts. Two types of dislocation are observed, grain boundary dislocations, which accommodate the misorientation between neighboring grains, and dislocations pinned within the bulk of the magnesium oxide grains. Neither of these has been reported previously, although strain contrast, which is probably due to dislocations, is evident on careful inspection of micrographs published by Lunsford *et al.* (*24*). The edge dislocations are line defects which run through the bulk of the grains and are classified as belonging to the type $\frac{1}{2}\langle 110\rangle$ (*32*). A charged region results where a dislocation emerges at the surface of a magnesium oxide crystallite. This is either an anion or a cation vacancy.

The dislocations are a direct consequence of the presence of lithium in the catalysts, since none have been observed in our extensive study of undoped magnesium oxide samples prepared from a variety of precursors, and it is interesting that similar defects are observed in the gold-doped catalysts. The dislocations are immobile, suggesting pinning of the defect by lithium ion segregation to the dislocation core. Figure 11 schematically shows the point of emergence of the $\frac{1}{2}\langle 110\rangle$ dislocation at the {100} rock salt surface. It has previously been proposed that oxygen vacancies and $[Li^+O^-]$ centres constitute the active sites for methyl radical generation at the surface of lithium-doped magnesium oxide catalysts (*2*). Since we believe that lithium is pinned at the dislocation lines it is reasonable to suggest that $[Li^+O^-]$ entities occur at the point of emergence of the dislocations. Thus even with lithium-doped magnesium oxide there is a morphological basis for catalytic performance. In addition, lithium substitution for $Mg^{2+}$ in the lattice will cause an increased concentration of point defects, which may also be active sites for methane activation.

The micrographs of Fig. 7 suggest that there are other morphological changes associated with lithium doping which also need

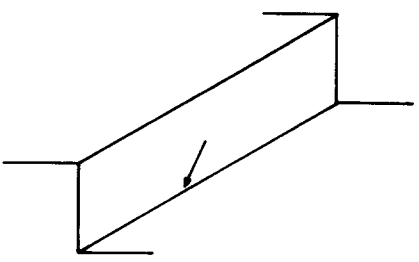

FIG. 10. Bottom step site.

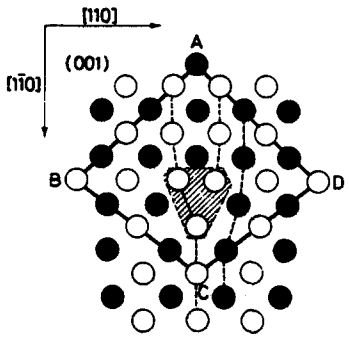


FIG. 11. Point of emergence of ½⟨110⟩ dislocation at the {100} surface of MgO. (●) $Mg^{2+}$, (○) $O^{2-}$.

to be considered. In comparison to the RR materials, the particles of the doped catalyst are quasi-spherical. As a result they will resemble the undoped, ex BC material, possessing a much higher number of corner and step sites than do the RR or ex OH catalysts. Aika *et al.* (*39, 40*), and Lunsford *et al.* (*41*), relying on a theoretical study of Mehandru *et al.* (*38*), have proposed that the improved selectivity of lithium-doped catalysts resulted from the removal of corner sites, which they suggest are nonselective. This is clearly not the case, as Lunsford *et al.* subsequently recognised (*24*), since the doped catalysts have a much higher density of corner sites than, for example, the RR catalysts. Although the presence of step sites may be beneficial, it seems more probable that the improved performance of the lithium-doped catalysts results from the presence of the $[Li^+O^-]$ centres: involvement of mobile lithium carbonate films cannot be ruled out.

Further evidence of the importance of emergent line defects in methane activation is provided by the results from magnesium oxide doped with gold, where dislocations similar to those found with Li/MgO catalysts are observed. However, in contrast to the Li/MgO materials, the Au/MgO catalysts give total oxidation products almost exclusively. The results given here are part of an extended study to be presented elsewhere, but it seems probable that isolated gold ions act as sites for the total combustion of $C_2$ hydrocarbons and that combustion rates and products are both different for ethane and ethene.

## CONCLUSIONS

Detailed study of magnesium oxide and lithium- and gold-doped magnesium oxide catalysts demonstrates the importance of the catalyst morphology and the defect structure of these materials in the oxidative coupling of methane. From studies of ex hydroxide and ribbon residue catalysts, which show similar morphology but very different cube size, we conclude that edge and corner sites are not catalytically significant. From examination of the ex BC material it is suggested that special, bottom step sites may be important for the selective coupling of methane. Examination of lithium-doped magnesium oxide catalysts has highlighted the role of emergent line defects in forming surface active sites, such as $[Li^+O^-]$, together with the increased number of point defects. It is clear that the selective activation of methane is a structure-sensitive reaction and that the role of morphology must be considered in the design of improved catalysts.

## ACKNOWLEDGMENTS

We thank Dr. Norman Parkyns for many stimulating discussions and British Gas PLC and the SERC for financial support. We also thank Midland Research Station, British Gas PLC, for carrying out the surface area determinations and the elemental analysis of the MgO and Li/MgO samples. Johnson Matthey and PLC are thanked for the loan of the gold compounds. Professor P. Turner is thanked for useful discussions. We are grateful to Dr. M. Raffiq H. Siddiqui for performing the XPS experiments.

## REFERENCES

1. Parkyns, N. D., *Chem. Br.* **26,** 841 (1990).
2. Lunsford, J. H., *Catal. Today* **6,** 235 (1990).
3. Ito, T., and Lunsford, J. H., *Nature (London)* **314,** 721 (1985).
4. Driscoll, D. J., Martir, W., Wang, S-X., and Lunsford, J. H., *J. Am. Chem. Soc.* **107,** 58 (1985).
5. Lin, C-H., Wang, J-X., and Lunsford, J. H., *J. Catal.* **111,** 302 (1988).
6. DeBoy, J. M., and Hicks, R. F., *J. Chem. Soc. Chem. Commun.*, 982 (1988).

7. Otsuka, K., and Komatsu, T., *J. Chem. Soc. Faraday Trans. 1* **83,** 1315 (1987).
8. Hutchings, G. J., Scurrell, M. S., and Woodhouse, J. R., *J. Chem. Soc. Faraday Trans. 1* **85,** 2507 (1989).
9. Emesh, I. T. A., and Amenomiya, Y., *J. Phys. Chem.* **90,** 4785 (1986).
10. Burch, R., Squire, G. D., and Tsang, S. C., *Appl. Catal.* **43,** 105 (1988).
11. Ashcroft, A. T., Cheetham, A. K., Foord, J. S., Green, M. L. H., Grey, C. P., Murrell, A. J., and Vernon, P. D. F., *Nature (London)* **344,** 319 (1990).
12. Nagamoto, H., Amanuma, K., and Inoue, K., *Chem. Lett.* 237 (1988).
13. Thomas, J. M., Ueda, W., Williams, J., and Harris, K. D. M., *Faraday Discuss. Chem. Soc.* **87,** 33 (1989).
14. Machida, K., and Enyo, M., *J. Chem. Soc. Chem. Commun.*, 1639 (1989).
15. Hatano, M., Hinsen, P. G., Shay Vines, K., and Lunsford, J. H., *J. Catal.* **124,** 557 (1990).
16. Yates, D. J. C., and Zlotin, N. E., *J. Catal.* **124,** 562 (1990).
17. Kalenik, Z., and Wolf, E. E., *J. Catal.* **124,** 566 (1990).
18. Cant, N. W., Lukey, C. A., Nelson, P. F., and Tyler, R. J., *J. Chem. Soc. Chem. Commun.*, 766 (1988).
19. Campbell, K.D., Morales, E., and Lunsford, J. H., *J. Am. Chem. Soc.* **109,** 7900 (1987).
20. Hutchings, G. J., Scurrell, M. S., and Woodhouse, J. R., *Chem. Soc. Rev.* **18,** 251 (1989).
21. Korf, S. J., Roos, J. A., Diphoorn, J. M., Veehof, R. H. J., van Ommen, J. E., and Ross, J. R. H., *Catal. Today* **4,** 279 (1989).
22. Sokolovskii, V. D., Buyevskaya, D. V., Plyasova, L. M., Litvak, G. S., and Uvarov, N.Ph., *Catal. Today* **6,** 489 (1990).
23. Le Van, T., Che, M., Kermarec, M., Louis, C., and Tatibouët, J. M., *Catal. Lett.* **6,** 395 (1990).
24. Lunsford, J. H., Cisneros, M. D., Hinson, P. G., Tong, Y., and Zhang, H-S., *Faraday Discuss. Chem. Soc.* **87,** 13 (1989).
25. Kung, H. H., "Transition Metal Oxides, Surface Chemistry and Catalysis," *Studies in Surface Science Catalysis, Vol. 45.* Elsevier, Amsterdam, 1989.
26. Moodie, A. F., and Warble, C. E., *J. Cryst. Growth* **10,** 26 (1971).
27. Moodie, A. F., Warble, C. E., and Williams, L. S., *J. Am. Ceram. Soc.*, 676 (1966).
28. Heinrich, V. E., *Surf. Sci.* **57,** 385 (1976).
29. Hargreaves, J. S. J., Hutchings, G. J., and Joyner, R. W., *Stud. Surf. Sci. Catal.* **61,** 155 (1991).
30. Goodman, J. F., *Proc. R. Soc. London A* **247,** 346, 1958.
31. Anderson, P. J., and Horlock, R. F., *Trans. Faraday Soc.* **58,** 1993 (1962).
32. Hull, D., and Bacon, D. J., "Introduction to Dislocations," 3rd ed., p. 128. Pergamon, Elmsford, NY.
33. Narayan, J., Abraham, M. M., Chen, Y., and Tohver, H. T., *Philos. Mag. A.* **38,** 247; 1989.
34. Turner, P. S., personal communication.
35. Hargreaves, J. S. J., Hutchings, G. J., and Joyner, R. W., *Nature (London)* **348,** 428 (1990).
36. Moggridge, G. D., Badyal, J. P. S., and Lambert, R. M., in press.
37. Hutchings, G. J., Scurrell, M. S., and Woodhouse, J. R., *Catal. Today* **6,** 399 (1990).
38. Mehandru, S. P., Anderson, A. B., and Bradzil, J. F., *J. Am. Chem. Soc.* **110,** 1715 (1988).
39. Iwamatsu, E., Moriyama, T., Takasaki, N., and Aika, K., *J.Catal.* **113,** 25 (1988); Cunningham, J., *Catal. Today* **2,** 557 (1988).
40. Moriyama, T., Takasaki, N., Iwamatsu, I., and Aika, K., *Chem. Lett.*, 1165 (1986).
41. Lunsford, J. H., Lin, C-H., Wang, J-X., and Campbell, K. D., *Mater. Res. Soc. Symp. Proc.* **111,** 305, 1988.